Faculty Mentor: Hays Rye
Princeton University
Department of Molecular Biology
Washington Road
Princeton, NJ 08544
609-258- 1707
hrye@princeton.edu

Current address: Texas A&M University
Associate Professor of Biochemistry & Biophysics
Phone: (979) 862-1123
Email: haysrye@tamu.edu

Graduate Student/Fellow: Kelly Krantz
Research Scientist

Grant title: Investigating the Mechanism of Clathrin Uncoating, a Key Step in Synaptic Transmission

Grant Number: 06-2914-SCR-E-0

Grant Period Covered by the Report: 6/15/07-1/31/08

Date of Submission of the Report: ***5/20/2010***

Publication: Burst analysis spectroscopy: a versatile single-particle approach for studying distributions of protein aggregates and fluorescent assemblies.

Puchalla J, Krantz K, Austin R, Rye H.

Proc Natl Acad Sci U S A. 2008 Sep 23;105(38):14400-5. Epub 2008 Sep 9.

1. Specific Aims and Significance

One of the main objectives in treating patients with spinal cord injuries (SCI) is to restore synapse function and plasticity. The function and plasticity of the synapse depends upon tight coupling between exocytosis of synaptic vesicles and endocytosis of the vesicle membrane[1]. One of the main forms of synaptic vesicle endocytosis is clathrin mediated endocytosis. Unfortunately, all of the steps involved in clathrin mediated endocytosis are not well understood despite the fact that mutations in many of the known proteins involved in clathrin mediated endocytosis lead to loss or impairment of synaptic transmission[2]. This prevents us from being able to gain a full understanding of synaptic transmission, and makes efforts to restore synaptic transmission in SCI patients extremely difficult.

During the past year, my efforts have focused on gaining a better understanding of synaptic transmission by examining clathrin uncoating, an essential process for fusion between synaptic vesicles and various cellular membranes. In particular I have focused on investigating the role that the 70kDa heat shock protein Hsc70 and its cochaperone auxilin play in clathrin uncoating.[3] In order to achieve this I have aimed to:

1. Purify and characterize fluorescently tagged *S. cerevisiae* clathrin baskets, and the uncoating proteins.
2. Reconstitute clathrin uncoating *in vitro* using only *S. cerevisiae* components.
3. Determine if the uncoating process is cooperative, by exploiting a novel single particle assay that can follow and measure the dynamics of the uncoating reaction.

2. Results and Progress

a. Purify and characterize fluorescently tagged S. cerevisiae clathrin baskets, and the uncoating proteins

Our lab has obtained a commercially available strain of *S. cerevisiae* where the clathrin heavy chain gene (CHC1) has been fused to GFP so that all Chc1p made by the yeast is fused to GFP at its C-terminus. We then purify assembled clathrin from this strain by modification of a previously established protocols involving differential centrifugation and gel filtration chromatography.[4] When the clathrin purified by this protocol is examined by electron microscopy, the vast majority of the field is a uniform population of approximately 30nm structures (figure 1). This is comparable to clathrin baskets which are purified and assembled in vitro using bovine clathrin[5-7]. Originally we had planned to use clathrin coated vesicles as an uncoating substrate however, clathrin baskets have served as a substrate for all previous biochemical studies of clathrin uncoating[8-12]. Also, the interactions between clathrin triskelia in a basket and a coated vesicle are believed to be identical, as is the mechanism used to disassemble such structures. Also we have found that large quantities of clathrin baskets, which are necessary for our experiments, are more easily obtained than clathrin coated vesicles. The clathrin baskets we purify show emission and excitation properties comparable to that of purified GFP. As stated in my original proposal I have also expressed and purified functional *S. cerevisiae* homolog's of Hsc70 (Ssa1p), and auxilin (Swa2p).

b. Reconstitute clathrin uncoating in vitro using only S. cerevisiae components

As described in my original proposal, we are able to monitor uncoating of clathrin baskets by looking at changes in the fluorescence burst intensity of samples. These changes are dependant upon the presence of Ssa1p, Swa2p, and ATP.

c. Determine if the uncoating process is cooperative, by exploiting a novel single particle assay that can follow and measure the dynamics of the uncoating reaction.

Over the past year we have measured the fluorescence burst intensity of clathrin baskets during the course of an uncoating reaction, and we have developed algorithms to calculate the change in burst height over time. Using these methods, we have found that variations in the concentration of Swa2p, within a physiological range do not affect the endpoint of the uncoating reaction. However, varying the concentration of Ssa1p within a physiological range has a large affect on the endpoint of an uncoating reaction (figure 2). To further investigate the affect of Ssa1p on the rate of the uncoating we are collecting data to obtain the rate of uncoating at various concentrations of Ssa1p. Preliminary data indicates that the rate of reaction increase with the concentration of Ssa1p (figure 3). However, additional concentrations of Ssa1p need to be examined to more fully map the functional dependence of the overall disassembly kinetics on Ssa1p concentration. We expect to have a large enough dataset for this plot within the next month, and the shape of this plot will reveal if uncoating is cooperative with respect to the concentration of Ssa1p. We are also in the process of calculating how the size of a fluorescence burst is proportional to the amount of GFP present on particle by calibrating burst intensity with free GFP. We hope to use this information to calculate the number of clathrin triskelia present on an uncoated piece of clathrin basket. This will allow us to determine if uncoating proceeds a single triskelia at a time, or if the basket breaks up into multi-triskelia fragments.

3. Discussion.

By determining is the uncoating reaction is cooperative with respect to the concentration of Ssa1p, and the number of triskelia present in an uncoated fragment, we hope to be able to distinguish between several models of uncoating. One possible model is that uncoating precedes one triskelion at a time, and removal of triskelia does not affect the stability of those remaining in the coat. The second model is that each triskelia is released one at a time, however once one triskelia is released the neighboring triskelia become less stable, and the probability of their release increases. The final model is that the coat is broken down into multi-triskelia fragments that are then further disassembled into smaller fragments. In the first model the uncoating would proceed in a linear fashion. In the second model the uncoating would proceed in an exponential fashion. In the third model the uncoating could proceed in either a linear or exponential fashion. We hope to have enough data to make this distinction in the next two months, and have already begun writing a manuscript describing our work, which will increase our understanding of the mechanism of clathrin coat disassembly. This information will further enhance our understanding of synaptic transmission and bring us closer to being able to manipulate, and/or recreate the synaptic transmission process in individuals with spinal cord injuries.

A

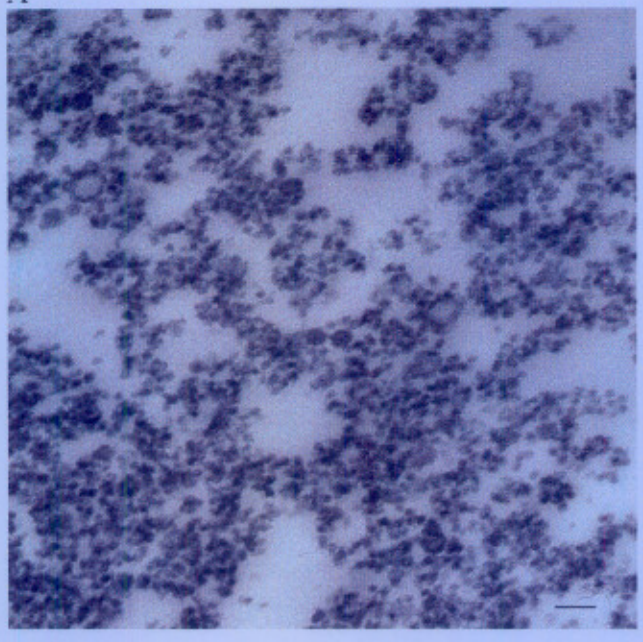

B

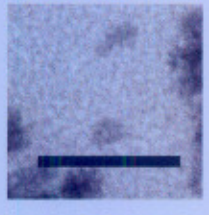

Figure 1. Negatively Stained Electron-microscopy Images of Purified Clathrin Baskets. Scale bar is 100nm **a,** full field image **b,** zoom

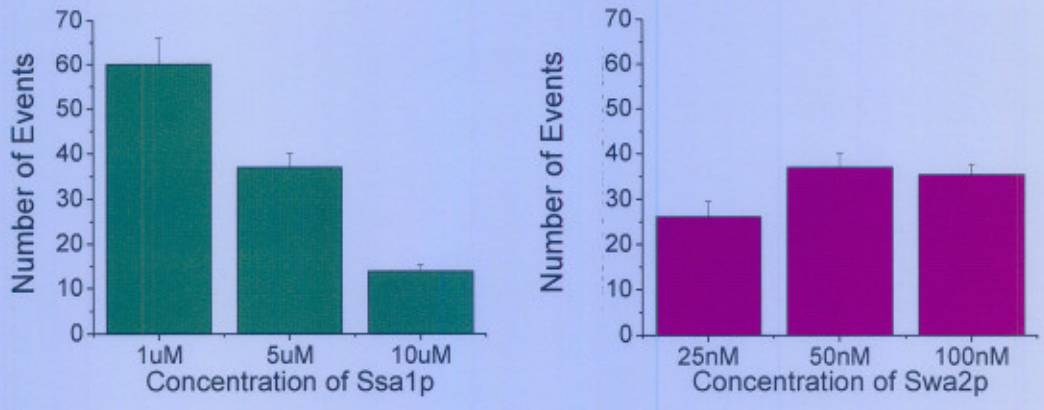

Figure 2 The uncoating reaction endpoint depends on the concentration of Ssa1p. Uncoating reactions were done with 2mM ATP, 10mM $MgCl_2$, and 50nM Swa2p with varied concentrations of Ssa1p or 5uM Ssa1p with varied concentrations of Swa2p. The number of fluorescence burst in the final 40sec were counted, error bars represent the standard error of the mean between three traces.

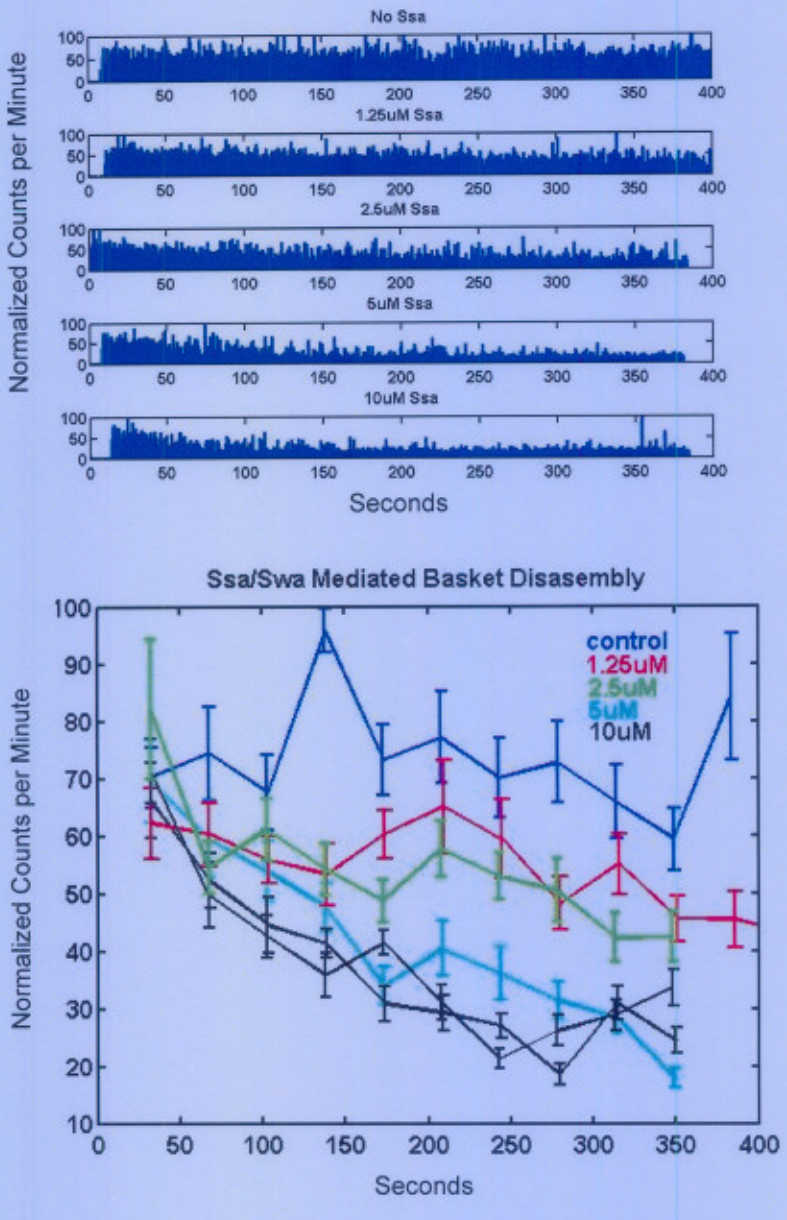

Figure 3 Increasing Concentrations of Ssa1p increase the rate at which fluorescence burst intensity decreases over time. **a**, Fluorescence burst traces of a sample of clathrin baskets with 50nM Swa2p, 2mM ATP, and varying concentrations of Ssa1p. As the uncoating reaction proceeds the baskets are broken into smaller pieces which have fewer triskelia and therefore produce a less intense fluorescence burst. Larger bursts disappear more quickly when higher concentrations of Ssa1p are present. **b,** Fluorescence burst traces were divided into 40sec bins and 25% of the bursts with the highest intensity were selected. The average of this 25% was then plotted versus time. Error bars represent the standard error of the mean between the 25% most intense peaks per bin.

1. Zinsmaier, K. E. & Bronk, P. Molecular chaperones and the regulation of neurotransmitter exocytosis. Biochem Pharmacol 62, 1-11 (2001).
2. Brodin, L., Low, P. & Shupliakov, O. Sequential steps in clathrin-mediated synaptic vesicle endocytosis. Curr Opin Neurobiol 10, 312-20 (2000).
3. Kirchhausen, T. Clathrin. Annu Rev Biochem 69, 699-727 (2000).
4. Mueller, S. C. & Branton, D. Identification of coated vesicles in Saccharomyces cerevisiae. J Cell Biol 98, 341-6 (1984).
5. Fotin, A. et al. Structure of an auxilin-bound clathrin coat and its implications for the mechanism of uncoating. Nature 432, 649-53 (2004).
6. Fotin, A. et al. Molecular model for a complete clathrin lattice from electron cryomicroscopy. Nature 432, 573-9 (2004).
7. Heuser, J. & Steer, C. J. Trimeric binding of the 70-kD uncoating ATPase to the vertices of clathrin triskelia: a candidate intermediate in the vesicle uncoating reaction. J Cell Biol 109, 1457-66 (1989).
8. Prasad, K., Barouch, W., Greene, L. & Eisenberg, E. A protein cofactor is required for uncoating of clathrin baskets by uncoating ATPase. J Biol Chem 268, 23758-61 (1993).
9. Pishvaee, B. et al. A yeast DNA J protein required for uncoating of clathrin-coated vesicles in vivo. Nat Cell Biol 2, 958-63 (2000).
10. Gao, B. C., Biosca, J., Craig, E. A., Greene, L. E. & Eisenberg, E. Uncoating of coated vesicles by yeast hsp70 proteins. J Biol Chem 266, 19565-71 (1991).
11. Gao, B., Greene, L. & Eisenberg, E. Characterization of nucleotide-free uncoating ATPase and its binding to ATP, ADP, and ATP analogues. Biochemistry 33, 2048-54 (1994).
12. Gao, B., Emoto, Y., Greene, L. & Eisenberg, E. Nucleotide binding properties of bovine brain uncoating ATPase. J Biol Chem 268, 8507-13 (1993).

Journal List > Proc Natl Acad Sci U S A > v.105(38); Sep 23, 2008

Proc Natl Acad Sci U S A. 2008 September 23; 105(38): 14400–14405. PMCID: PMC2567176
Published online 2008 September 9. doi: 10.1073/pnas.0805969105.

Physics, Biophysics

Burst analysis spectroscopy: A versatile single-particle approach for studying distributions of protein aggregates and fluorescent assemblies

Jason Puchalla,[*†‡] Kelly Krantz,[†] Robert Austin,[*‡] and Hays Rye[†‡]

Departments of *Physics and
[†]Molecular Biology, Princeton University, Princeton, NJ 08544
[‡]To whom correspondence may be addressed. E-mail: puchalla@princeton.edu , Email: austin@princeton.edu , or ; Email: hrye@princeton.edu
Contributed by Robert Austin, June 27, 2008

Author contributions: J.P., R.A., and H.R. designed research; J.P., K.K., and H.R. performed research; J.P. and K.K. contributed new reagents/analytic tools; J.P. and K.K. analyzed data; and J.P., K.K., R.A., and H.R. wrote the paper.

Received December 31, 2007

ABSTRACT

Many essential cellular functions depend on the assembly and disassembly of macromolecular complexes. The size, form, and distribution of these assemblies can be heterogeneous and complex, rendering their detailed characterization difficult. Here we describe a simple non-correlation-based method capable of directly measuring population distributions at very low sample concentrations. Specifically, we exploit the highest signal-to-noise light bursts from single fluorescent particles transiting a confocal excitation spot to recursively determine the brightness and size distribution of complex mixtures of fluorescent objects. We refer to this method as burst analysis spectroscopy (BAS) and demonstrate the sensitivity of this technique by examining the free-solution, time-resolved distribution of assembled protein aggregates by using two fluorescently labeled proteins: the aggregation-prone, chaperonin-dependent, folding model protein ribulose-bisphosphate carboxylase/oxygenase (RuBisCO), and an amyloidogenic fragment of the yeast prion protein Sup35. We find that the assembly kinetics of both proteins display complex multimodal behavior not readily quantifiable with other methods.

Keywords: aggregation, fluorescence spectroscopy, microfluidics

The assembly and disassembly of macromolecular complexes is a fundamental property of cellular biology. Understanding the dynamics of molecular assemblies such as viral capsids, transport vesicle coats, cytoskeleton assemblies, and multienzyme complexes is both essential and challenging. A key and especially demanding example is protein aggregation. In some cases, aggregation of proteins can trigger severe cellular dysfunction and disease (1, 2). In general, protein aggregation is initiated by the spontaneous formation of a limited population of small oligomers, which eventually, and often explosively, grow into a heterogeneous population of assembled states that can span several orders of magnitude in size (3). Additionally, the precise aggregation pathway followed can be an exquisitely sensitive function of environment (3, 4) such that shear forces, fractionation, or solvent conditions experienced during measurement can dramatically perturb the population distribution under study. The inherent heterogeneity of an aggregating protein sample suggests that a single-particle method capable of resolving complex species distributions, while minimally perturbing a sample under study, would be an especially powerful complement to current approaches.

One of the most versatile general strategies for observing single particles and detecting rare molecular events involves the optical fluorescence labeling of a target sample. Fluorescence labeling has proven to be a highly sensitive method for the single-particle detection of protein aggregates in a variety of assays (5, 6). Techniques that specifically monitor fluctuations in fluorescence intensity (7–10) are well suited to the analysis and characterization of small molecules or mixtures of only a few species. However, these established methods are not, in general, well suited for the analysis of the early stages of protein aggregation where the oligomer concentration is low and the species distribution is highly diverse in size and concentration. Large, slow moving, and potentially rare aggregates possessing very high specific fluorescence intensities can dominate diffusion-based measurements. This fact makes it difficult to determine a meaningful average species concentration for a heterogeneous sample by using standard fluctuation methods. Likewise, the wide range of intensity fluctuations associated with low concentrations of bright particles diffusing through an excitation volume is not well described by a simple Poisson distribution (11). More complex, multiparameter methods using intensity, lifetime, anisotropy, and spectral range (12, 13) have also been demonstrated by combining time-correlated single-photon counting measurements with fluorescence correlation spectroscopy.

Here we present a simple and complementary approach to quantifying a broad distribution of fluorescently labeled species at low concentration. Although the experimental approach retains the advantages of being able to perform traditional photon counting and coincidence detection (14, 15), the approach does not require correlation analysis or a precision scanning stage to determine the population distribution. It is intended for the exploration of very low sample concentrations such as those inherent in aggregate formation and disassembly. The particle brightness distribution can be explored over several orders of magnitude with minimal sample perturbation. In this presentation, our analysis is restricted to high signal-to-noise bursts from particles containing multiple fluorescent probes per particle so that photon shot noise can be neglected. We demonstrate the ability to map the kinetic species landscape for both a model CO_2-fixing enzyme, ribulose-bisphosphate carboxylase/oxygenase (RuBisCO) from *Rhodospirillum rubrum*, and the purified yeast prion protein Sup35. In both cases, the distinct dynamics of a subpopulation of rapidly growing aggregates highlights the utility of this single-particle approach.

RESULTS

The method presented here requires flowing fluorescently labeled particles through an excitation volume and measuring the photon bursts recorded by a sensitive detector. A significant difference between this approach and scanning fluorescence correlation spectroscopy (FCS) techniques (16, 17) is that our semiempirical method does not rely on particle diffusion. We chose to build a standard dual-color confocal microscope from modular components (Fig. 1*A*) to demonstrate the feasibility of constructing a low-cost (<$20,000 without excitation source) system capable of quantifying a fluorescent distribution. An inexpensive motorized open-loop stage rotates the sample at a fixed rate.

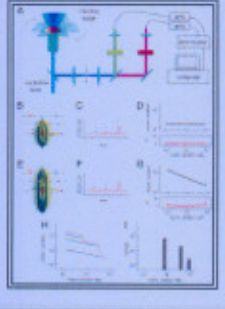

Fig. 1.

The fluorescence burst distribution of a sample flowing although a non-Gaussian excitation volume. (*A*) Schematic of the apparatus used for burst analysis spectroscopy (BAS). Burst measurements were conducted with a standard confocal microscope fitted (more ...)

In a typical measurement, each labeled particle that transits through the excitation volume produces a fluorescent burst whose peak intensity value is determined, then stored for subsequent analysis. The sample scan rate is chosen to be much faster than the particle transit rate due to free diffusion but much slower than the fluorescent

excitation/de-excitation rate [see supporting information (SI) *Methods*]. For a typical confocal excitation profile (18) under these conditions, the peak intensity of each burst occurs just as the particle crosses the central plane of the excitation volume where the laser intensity is highest (Fig. 1 *B* and *C*). Thus, a histogram of the excitation intensities corresponding to the central plane of the excitation volume is equivalent to a noiseless model of the burst amplitude histogram of a single, uniformly bright species transiting this volume. Because there is a much greater probability of a particle crossing the beam at a region of low excitation intensity, the raw burst data will contain a large number of small-amplitude events. To compensate, the collected burst data can be logarithmically binned in amplitude. The application of this binning strategy to the intensities of the central plane of a Gaussian excitation profile yields a model that predicts that the burst amplitude histogram of a single fluorescent species will be flat (Fig. 1*D*). Importantly, the addition of a second, noninteracting species of a different intrinsic brightness should then lead to no more than an offset in the histogram up to the maximum burst amplitude of the new species. In other words, the burst amplitude histogram will change in a manner identical to the cumulative distribution. For a more realistic combined Gaussian–Lorentzian (GL) excitation model (18), logarithmic binning yields a histogram that is no longer the flat, cumulative distribution but is well approximated by a power law (Fig. 1 *E*, *F*, and *G*). Once again, however, additional noninteracting species of differing intrinsic brightnesses lead to offsets in the histogram up to the maximum burst amplitude of each new species (Fig. 1 *H* and *I*).

In general, a particle distribution is likely to be composed of multiple subspecies each possessing a different intrinsic brightness. To recover the species number distribution, one needs to differentiate dim species passing through the center of the excitation profile from bright species passing through the edge of the profile. This problem can be solved by constructing a corrected burst histogram by using information about the most highly fluorescent species detected in the course of a measurement. If all particles cross the excitation beam profile at random and uncorrelated positions, the most intense burst detected can, in principle, come only from the most highly fluorescent objects passing through the center of the excitation volume. The average number of bursts contributing to each of the lower intensity bins from the passage of the most fluorescent species through regions of lower excitation intensity can be calculated by using a model (18, 19) or a direct measurement of the beam profile. After the contribution to each histogram intensity bin from the most fluorescent species is removed, any bursts that remain in the second brightest bin can come only from a second, but slightly dimmer, fluorescent species. This procedure can then be repeated. Thus, each intensity bin can be corrected for the average contribution coming from each object of greater fluorescence intensity to

yield a corrected histogram that estimates the number distribution. We have derived a recursion formula that implements this process. The corrected histogram provides a straightforward measure of changes in species number and brightness even when the volume of the excitation profile is not precisely known. In total, we refer to this burst detection strategy as burst analysis spectroscopy (BAS).

BAS Numerical Analysis.

BAS analysis leads to an estimate of the fluorescence intensity distribution with an intrinsic resolution and dynamic range set by the binning choice. Whereas the number of independent fluorescent species is typically unknown *a priori*, BAS can explore the fluorescence distribution in increasing detail by binning the burst amplitude data into smaller intensity bins at the cost of increasing the noise per bin. In this work, typically 15 bins covering two orders of magnitude in photon rate were collected in ≈5 min. The number of bins was chosen to ensure that the average intensity variance between adjacent bins exceeded the average photon shot noise within a bin (see *SI Methods*).

On the basis of the results shown in Fig. 1*g* and the reasoning outlined above, we begin by assuming that a single monodisperse fluorescent species will lead to a burst amplitude histogram $H_1(I)$ that can be modeled as $H_1(I) = a_1T(I)$. The characteristic function, $T(I)$, is determined by the shape of the microscope excitation profile, a_1 is a constant of proportionality, and I does not exceed some maximal burst amplitude I_1 that depends on the sample and excitation power. The functional form of $T(I)$ will depend on the shape of the excitation profile but must be confirmed to be independent of I_1 and excitation power. For a 2D Gaussian profile, it can be shown that $H_1(I) = a_1/I$ so that logarithmic binning in amplitude leads to a flat histogram (see *SI Methods*). For a Gaussian–Lorentzian profile as in the case of our system, $T(I)$ is well approximated by a power law. Extending this to a case where the fluorescence species distribution is more complex and extends over multiple intensity bins implies a total histogram $H(I) = \Sigma H_i(I)$.

In general, once the actual function $T(I)$ is known, the burst amplitude histogram can be corrected to yield an estimate of the number distribution. This correction is carried out as follows. The events in the brightest measured histogram bin m_N are composed of only the brightest bursts and can be used to determine the amplitude of $H_N(I)$ because no dimmer species can contribute to this bin. That is, $m_N = H_N(I_N) = a_NT(I_N)$, where I_N is the average burst amplitude of the Nth bin. The second brightest bin measurement, m_{N-1}, is the sum of $H_N(I_{N-1})$ and $H_{N-1}(I_{N-1})$. In general, the ith measurement $m_i = T(I_i)\Sigma_{j=i}^{N} a_j$ and the proportionality constant of the ith bin is $a_i = m_i/T(I_i) - \Sigma_{j=i+1}^{N}a_j$. Only bins brighter than the ith bin contribute to the sum. The corrected number of elements in the ith bin $n_i = m_i - T(I_i)\Sigma_{j=i+1}^{N}a_j$. In practice, once the appropriate form of $T(I)$ is found from a calibration measurement, the raw photon rate

histogram data m_i is fit to a model (here denoted as q) such that $q_i = T(I_i)\Sigma_{j=i}^{N} a_j w_j$ where w_j is an N-element masking vector that is nonzero only for $j \geq i$ and accounts for the conditional sum. Fitting is done by using the weighted least-squares fitting algorithm *fit* in Matlab where the weighting is uniform wherever the binary masking vector is nonzero. The number of free parameters a_i fit is the same as the number of input data points (bins). The required correction to the fit model is $\Delta_i = T(I_i)\Sigma_{j=i+1}^{N} a_j w_j$. The corrected histogram is then $H^{\text{corrected}}(I_i) = (q_i - \Delta_i)$ for $i < N$ and $H^{\text{corrected}}(I_N) = q_N$. Knowledge of the mean flow rate, excitation geometry, and time of data collection allows conversion of this number histogram into concentration (see *SI Methods*).

A Fluorescence Distribution with Multiple Mixed Species.

To demonstrate that BAS can robustly extract brightness and size distribution information from a heterogeneous sample, we first examined samples of polystyrene fluorescent nanospheres. We used three different samples of nanospheres (49 nm, 63 nm, and 100 nm), into each of which the same fluorescent dye was embedded. The uncorrected and corrected burst amplitude histograms for each bead sample are shown in Fig. 2 *A–C*. The uncorrected histograms display two important features: (*i*) a power-law dependence in photon rate that matches what would be expected for the GL excitation profile of our instrument and (*ii*) a characteristic roll-off at higher brightness caused by the inherent size variation of each nanosphere sample (specified as 10–15%). We find that, once intensity and integral normalized, the shape of a burst histogram is independent of excitation power, suggesting that photon-counting statistics do not affect the measurement of particle size distributions under these analysis conditions (Fig. 2*D*). We next compared the experimentally measured nanosphere distributions to the results of a simulation analysis. We assumed that the fluorescence intensity of the nanospheres varies linearly with volume and that the dispersion in nanosphere size is normally distributed around a mean size. The linear relationship between bead size and fluorescence intensity was confirmed by measuring the fluorescence intensity ratio of the different nanospheres at high concentration and equivalent excitation power (data not shown). A series of Monte-Carlo simulations was performed by using a uniform sampling of the central plane of a GL excitation volume. This analysis demonstrates that BAS can measure the size variation of a single fluorescent species to better than 5% (Fig. 2*D*, dashed lines; 11 ± 3% for the 100-nm nanosphere sample).

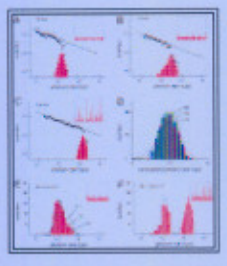

Fig. 2.

Resolving mixed populations of fluorescent nanospheres. Dilute solutions of 49-nm (*A*), 63-nm (*B*), and 100-nm (*C*) fluorescent nanospheres were independently examined by BAS. cps, counts per second. The uncorrected (black dots) and corrected (red bars) (more ...)

We next examined how well BAS can extract distribution information from mixtures of fluorescent nanospheres. We used two nanosphere mixtures for this analysis: (*i*) 49 nm plus 63 nm at a mixing ratio of 5:1 and (*ii*) 49 nm plus 100 nm at a mixing ratio of 1:1. In both cases, the presence of two distinct species, as well as the relative brightness, concentration, and population distribution of each species, can be determined from the corrected histograms (Fig. 2 *E* and *F*). Stringent simulation analysis confirms that BAS can robustly detect differences in mixed samples, even when particles differ in size or concentration by less than a factor of 2 (Fig. 2 *E* and *F*, dashed lines). For these simulations, the same number of events detected in each mixing experiment was used for each simulation ($n_{49/100}$ = 4,447, $n_{49/63}$ = 2,879). The simulation model accounts for both the expected distribution of fluorescent nanospheres and for Poisson noise (see *SI Methods*). Importantly, the experimentally measured amplitude distributions very closely match the distributions predicted by this analysis (Fig. 2 *E* and *F*; $R_{49/63}^2$ = 0.985, $R_{49/100}^2$ = 0.965). All measurements were repeatable to within sampling noise.

As sample complexity increases, the inherent constraints of photon burst detection, instrument noise, and the inescapable low number sampling of high brightness events combine to place limits on the ability of BAS to detect and discriminate different populations. However, a practical dynamic range of BAS measurements and the method's power to discriminate between distributions can be demonstrated by examining the corrected photon rate histogram calculated from a simulated, complex population of fluorescent particles. The equilibrium ensemble distribution of a simple, diffusion-limited aggregating system has previously been modeled as a power law with an associated spectral index (20). Hence, we compared the BAS estimated brightness distributions from a burst simulation with the original underlying power law distribution used to create the simulated bursts. The results of the analysis and the underlying power laws expected are shown in Fig. 3. Estimated distributions (here corrected for logarithmic binning) for three spectral indices demonstrate excellent agreement [$R_{n=0}^2$ = 0.985 (X), $R_{n=-1}^2$ = 0.990 (O), $R_{n=-2}^2$ = 0.997 (+)] with the original distributions (dashed lines). BAS measurement sensitivity wanes faster for low photon rate events when the source distribution is more uniform. This is due to the faster increase in relative sample variance in the lower intensity bins from brighter members

of the population. A practical limit for BAS measurements such as those presented here is thus approximately two orders of magnitude in photon rate.

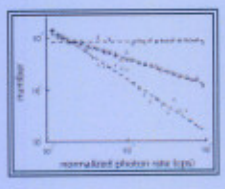

Fig. 3.

Characterization of continuous particle distributions. The number distributions of various fluorescent populations were analytically modeled and compared with BAS analysis of simulated burst data. Predictions for three different power law distributions (more ...)

Measurement of Population-Resolved Aggregation Kinetics.

BAS not only provides a simple method for studying the species distribution of complex, fluorescent macromolecular systems but also provides a way to follow the temporal evolution of these systems. We therefore examined the capacity of BAS to characterize the aggregation dynamics of two model proteins that display highly divergent aggregation behavior: (*i*) the amorphously aggregating globular enzyme RuBisCO and (*ii*) an amyloid-forming fragment of the yeast prion protein Sup35.

The CO_2-fixing enzyme RuBisCO from *R. rubrum* is a well established model substrate for the study of molecular chaperone-dependent protein folding (21, 22). We created a tetramethylrhodamine (TMR)-labeled, metastable, and aggregation-prone RuBisCO folding intermediate by using previously described procedures (see *Materials and Methods*). Small aliquots (25 μl) of the nonnative RuBisCO monomer at 4°C were withdrawn, warmed to 22°C for different times to trigger aggregation, and then diluted to low concentrations to slow the aggregation reaction during data acquisition. BAS measurements were taken for five different incubation times ($n_{60\ min}$ = 1,028, $n_{20\ min}$ = 1,175, $n_{5\ min}$ = 1,168, $n_{1\ min}$ = 824, $n_{30\ sec}$ = 664) at 22°C and demonstrated dramatic shifts in the RuBisCO aggregate population distribution as a function of aggregation time (Fig. 4). A subpopulation of small aggregates characterized by very rapid growth was detectable in the first minute of the aggregation reaction. Within 5 min, a different and slower growing population then appeared to partially catch up. After 20 min, the distribution had largely stabilized. Based upon a detailed calibration analysis (see Fig. S1), the RuBisCO aggregates detected range from 5 to 500 RuBisCO monomers in size and did not exhibit significant quenching or quantum yield changes. The number distributions shown (Fig. 4*B*) are presented as the apparent concentration of aggregated particles (see *SI Methods*).

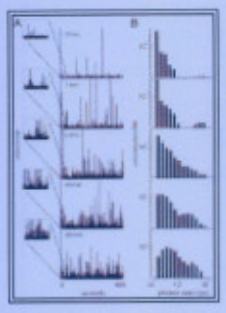

Fig. 4.

Detection of subpopulations of protein aggregates with distinct growth kinetics. The aggregation dynamics of the fluorescently labeled model protein RuBisCO were examined at 22°C. (*A*) Aggregate burst amplitudes are shown for five different aggregation (more ...)

We next examined the oligomerization and β-amyloid conversion of a fragment of the yeast prion protein Sup35. Sup35 is a well established yeast model for studying the formation, infectivity, and propagation of prions (23, 24). The glutamine-rich, amino-terminal to middle fragment of Sup35 (Sup35NM) has been shown to mediate the conversion of Sup35 to amyloid-like fibrils linked to prion conversion and propagation (25). When a sample of purified Sup35NM was diluted out of strong denaturant into agitated aqueous buffer, light-scattering measurements showed a concentration-dependent lag phase followed by a nearly concentration-independent sigmoidal polymerization phase characteristic of this protein (23).

We used BAS and the small organic dye thioflavin T (ThT) to track the formation of Sup35NM oligomers. ThT displays only weak fluorescence in free solution or in the presence of unstructured, amorphous aggregates but becomes highly fluorescent upon binding to the organized β-sheet structure found in amyloid fibrils (26). We chose to use this small noncovalent ligand to follow Sup35NM conversion for two reasons: (*i*) based upon BAS measurements with a covalently attached fluorescent dye, no more than 2–5% of the total Sup35NM forms detectable multimeric assemblies (data not shown; a similar conclusion, based on centrifugation analysis, has been previously reported in ref. 23) and (*ii*) the use of a noncovalent, property-specific ligand allowed us to explore the use of BAS to isolate and examine the dynamics of distinct subpopulations within a larger total population. Because the functional relationship between ThT fluorescence and oligomer size is unknown, we do not attempt to convert ThT fluorescence brightness to monomer number. Although size or aggregate type-induced changes in the ThT quantum yield prevents this more detailed analysis, previous work and the monotonic increase in bulk ThT fluorescence (Fig. 5*A*) imply that Sup35NM oligomer size and ThT fluorescence intensity are directly related. Thus the measured number distribution can still be used to monitor distinct, well separated populations.

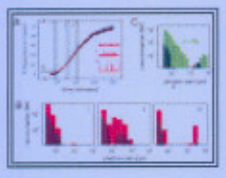

Fig. 5.

The formation of β-amyloid character in oligomers of the yeast prion protein Sup35NM. (*A*) A bulk fluorescence curve of Sup35NM (0.5 μM) undergoing continuous stirring in the presence of 1 μM thioflavin T is shown. The fluorescence (more ...)

At different times along the trajectory of a bulk Sup35NM assembly reaction (followed by ThT fluorescence), samples were extracted and subjected to BAS analysis (Fig. 5*B*; n_i = 1,396, n_{ii} = 1,226, n_{iii} = 566). During the lag phase in the reaction, no ThT fluorescence bursts were detectable. As the bulk ThT fluorescence of the sample began to increase, we observed a distinct population of Sup35NM oligomers that bound ThT. At longer times, a subset of the population displayed a dramatic increase in ThT binding. Surprisingly, however, only a fraction of the Sup35NM that bound ThT appeared to be competent to form large-scale structures. A subpopulation of small ThT-positive oligomers appeared to stall or progress toward larger assemblies only very slowly. The corrected number distribution (shown as concentration in femtomolar) at this stage of Sup35NM assembly (Fig. 5*B iii*) is clearly composed of two distinct populations. Importantly, the detection of the smaller sized, slow-growing subpopulation was not dependent on the bin size used in the analysis; a range of more and less coarse binning showed the same overall form of the corrected brightness histogram, as well as consistent scaling of the object number per bin. To establish whether the smaller species were transiently populated through an unstable side process, we repeated the aggregation measurement and allowed the polymerization to proceed to completion (>4 h; based on light scattering and bulk ThT fluorescence under these conditions; n = 492). A sample of the reacted solution was then diluted 100-fold and analyzed by BAS under identical conditions. Because of agitation-induced shearing, precipitation before the BAS measurement and significant dilution, we anticipated that large fibrils would be absent or not detectable. Remarkably, comparison of the Sup35NM oligomer distribution at midreaction to the extended incubation endpoint demonstrated that the smaller, slow growing subpopulation increased modestly in size and number without disappearing or fully converting to larger oligomers (Fig. 5*C*).

DISCUSSION

Macromolecular assemblies can populate a diverse array of structural states. Essential biological processes may be heavily influenced by the precise distribution of macromolecular states or by rare, highly active subspecies that are present at very low concentrations (27, 28). Under these conditions, it can be difficult or even impossible using standard techniques to quantify the population distribution of a macromolecular assembly or to track the development of a key subpopulation. Here

we have presented a single-particle fluorescence method we refer to as BAS that overcomes many of these limitations and permits the rapid, minimally perturbative, free-solution analysis of complex macromolecular distributions. BAS does not rely on diffusion to quantify the number distribution of a heterogeneous population of fluorescently labeled macrostructures and is computationally and experimentally simple. Because of its speed and simplicity, BAS provides a methodologically straightforward way to quantify the kinetics of macromolecular assembly or disassembly without perturbing the system by fractionation. Furthermore, site-specific probes are not required to explore subpopulation dynamics and, thus, the results serve to complement existing cross-correlation techniques (5, 15). While we have shown one aggregation example (RuBisCO) where fluorophore quenching does not deleteriously affect BAS analysis, quenching will change the functional relationship between burst intensity and aggregated size. However, as long as the correspondence between burst intensity and aggregate size or functional form is well behaved, it is still possible to track distinct subpopulations through the measured number distribution. We have applied this method to the yeast prion fragment Sup35NM.

In this first application of BAS, we have shown that it is possible to recover the expected species distribution of a mixed solution of fluorescent nanospheres in excellent agreement with numerical simulations. In addition, two substantially different protein aggregation processes were examined to demonstrate the ability to detect and quantify the formation of macromolecular subpopulations. In both cases, we detect complex, multimodal population distributions not readily observable with other methods. Given the fundamentally different physical endpoints of these two protein aggregation reactions (amorphous aggregate and amyloid fibril), our results suggest that multipopulation kinetics may be characteristic of a wide range of protein aggregation reactions. Additional studies will be required to examine the generality of these observations and the physiological importance of this shared multimodal behavior. A more detailed understanding of how solution conditions affect the temporal evolution of aggregated protein states should prove highly valuable in the development of general physical models for predicting and controlling the kinetics of protein aggregation and amyloid formation (28, 29). For example, the detection and study of low-order, prefibrillar intermediates in the protein aggregation reactions associated with diseases such as Alzheimer's and Huntington's are likely to be key to a complete understanding of these disorders (1, 2).

MATERIALS AND METHODS

Protein Preparation.

RuBisCO from *R. rubrum* was expressed and purified as described in ref. 22. Native RuBisCO was labeled at a single exposed Cys residue (C58) with tetramethylrhodamine-5-iodoacetamide as described in ref. 22. RuBisCO aggregation was initiated from a nonnative intermediate state of the protein that is stably populated at low temperature and low ionic strength (22). In brief, native RuBisCO labeled with TMR was denatured in 8 M acid-urea for 30 min at 22°C. The denatured protein was then rapidly diluted (350-fold) to a final concentration of 200 nM into buffer A (50 mM Hepes, pH 7.6/10 mM KOAc/5 mM $Mg(OAc)_2$/2 mM DTT) at 4°C. Using chilled pipette tips, 25-μl aliquots of the cold, nonnative protein sample were withdrawn and placed into a vial at 22°C to initiate aggregation. At different times, the sample was then diluted (20-fold) in buffer A at 22°C to suspend aggregation. Samples were then subjected to immediate BAS analysis. All sample containers were blocked with 10 mg/ml BSA, rinsed with ultrapure deionized water, then air dried before use.

Sup35NM was expressed and purified as described in refs. 24 and 25. Sup35NM assembly reactions were conducted essentially as described in ref. 24. In brief, nonnative Sup35NM in denaturation buffer (50 mM Mes, pH 6.0/4 M urea/4 M guanidinium·HCl/50 mM NaCl/5 mM 2-mercaptoethanol) was rapidly diluted (70- to 200-fold) into a 3-ml casein-blocked quartz cuvette at 22°C containing buffer B (40 mM Hepes, pH 7.4/150 mM KCl/20 mM $MgCl_2$/1 mM DTT) and 1 μM thioflavin T (ThT). The final Sup35NM concentration was varied between 0.5 and 1.5 μM. The sample was subjected to continuous stirring with a spin vein and magnetic stirrer (200 and 500 rpm) to facilitate fibril growth. The extent of fibril assembly was monitored in real time by ThT fluorescence (excitation 457 nm; emission 483 nm). Aliquots (100 μl) were withdrawn from the sample cuvette at different incubation times and placed on casein-blocked coverslips for immediate BAS analysis.

Single Particle Detection Platform.

All data were collected by using a custom-built confocal microscope built on a Nikon TE2000 microscope base and coupled to an argon-ion laser (Spectra-Physics Beamlok 2060-RMS) through a single-mode fiber. Average power was stable to better than 2% throughout all experiments. An acousto-optical tunable filter (NEOS model 6404010W) enabled color selection. For all experiments, a Nikon 60× N.A. 1.4 objective was used. We constructed a modular pinhole (50 μm) and dual-color filter assembly that attached to one of the microscope's side access ports. For all reported data, the output of this modular assembly was coupled to an avalanche photodiode (APD) detector (Perkin-Elmer SPCM-ARQ-12-FC) via multimode fiber optics. For all RuBisCO aggregation measurements, the 568-nm laser line excitation was chosen and emission was collected with a 605/50-nm bandpass filter. For experiments with

Sup35NM and ThT, 457-nm excitation was used and emission was monitored with a 505/50-nm bandpass filter. The beam waist diameter in the flow direction as determined from standard FCS measurements of tetramethylrhodamine (data not shown) was determined to be 0.4 μm for the green channel and 0.45 μm for the red channel. The instrument point spread function was also measured by axial scanning through 100-nm beads and confirmed the suitability of GL model assumptions. Fluorescent bead measurements were performed in both green and red bands, but because they are consistent only the red channel data are presented here. The APD output was time-stamped by a Flex01–12D hardware correlator (Correlator.com) connected to a standard PC via a USB-II communication link. This unit was primarily used to provide a time stamp during BAS measurements but also allowed for monitoring rotation speed through the fluorescence autocorrelation.

Protein samples were placed in a shallow well on BSA (10 mg/ml; for RuBisCO experiments) or casein (5% wt/wt; for Sup35 experiments) coated coverslips. Blocking times were either 30 min (casein) or 1 h (BSA). Coverslips were rinsed with deionized water and blown dry before well attachment. The wells, formed of PDMS silicone (Sylgard 184; Dow Corning), were ≈5 mm wide by 2 mm deep. Each well was covered before taking measurements to prevent evaporation. Coverslip assemblies were offset and rotated at 300–500 μm/s as measured at the excitation volume by using a custom torque motor assembly affixed to the objective. The rotation speed was calibrated optically by using a precision reticule. Fluorescent nanospheres were purchased from Duke Scientific as 1% solid suspensions. Typically, stock solutions were diluted by 10,000 to 100,000 depending on diameter to achieve 300–1,000 fM solutions. Nanosphere burst histograms similar to those shown in this article were also attained by using a two-photon microscope (data not shown).

A modified Lee filter (30) was used to identify individual bursts. These putative events were masked out and the background signal was determined then removed from the original data stream. Only bursts exceeding a lower signal-to-noise limit are retained (see *SI Methods*). The mean background signal was removed before isolating individual burst events for analysis. To estimate the fraction of multiparticle events, we considered the fraction of burst event pairs that occur closer in time than that required for a particle to cross the 2σ beam width (2.7 ms for 300 μm/s flow) by using an exponential rate model. Only data sets where this fraction was <2% were considered. Photon arrival time data were binned into 500- or 1,000-ms bins. Each isolated burst either was fit to a Gaussian profile to find its amplitude or the maximal value during the burst was used. These two methods yielded identical results to within experimental uncertainty, as expected for high signal-to-noise events. All analysis was carried out by using custom software written in Matlab 7.4.

SUPPLEMENTARY MATERIAL

Supporting Information

Click here to view.

ACKNOWLEDGMENTS.

We thank Drs. Jonathan Weissman and Sean Collins for the Sup35NM expression construct and technical assistance. We also thank Drs. Ned Wingreen, Chavela Carr, Don Winkelman, Nai Phuan Ong, and Edward Groth for helpful discussions and comments. Thanks to Stephan Thiberge for technical assistance and discussion of two-photon studies. This work was supported by grants from the National Institutes of Health (GM065421), National Science Foundation (DMR-0213706), and the New Jersey Commission on Spinal Cord Research (06A-004-SCR3).

FOOTNOTES

The authors declare no conflict of interes.

This article contains supporting information online at

www.pnas.org/cgi/content/full/0805969105/DCSupplemental.

REFERENCES

1. Chiti F, Dobson CM. Protein misfolding, functional amyloid, and human disease. *Annu Rev Biochem.* 2006;**75**:333–366. [PubMed]

2. Caughey B, Lansbury PT. Protofibrils, pores, fibrils, and neurodegeneration: Separating the responsible protein aggregates from the innocent bystanders. *Annu Rev Neurosci.* 1996;**26**:267–298. [PubMed]

3. Philo JS. Is any measurement method optimal for all aggregate sizes and types? *AAPS J.* 2006;**8**:E564–E571. [PMC free article] [PubMed]

4. Cromwell MEM, Hilario E, Jacobson F. Protein aggregation and bioprocessing. *AAPS J.* 2006;**8**:E572–E579. [PMC free article] [PubMed]

5. Bieschke J, et al. Ultrasensitive detection of pathological prion protein aggregates by dual-color scanning for intensely fluorescent targets. *Proc Natl Acad Sci USA.* 2000;**97**:5468–5473. [PMC free article] [PubMed]

6. Ban T, Goto Y. Direct observation of amyloid growth monitored by total internal reflection fluorescence microscopy. *Methods Enzymol.* 2006;**413**:91–102. [PubMed]

7. Giese A, et al. Single particle detection and characterization of synuclein co-aggregation. *Biochem Biophys Res Commun.* 2005;**333**:1202–1210. [PubMed]

8. Chen Y, Wei LN, Muller JD. Probing protein oligomerization in living cells with fluorescence fluctuation spectroscopy. *Proc Natl Acad Sci USA.* 2003;**100**:15492–15497. [PMC free article] [PubMed]

9. Muller JD, Chen Y, Gratton E. Resolving heterogeneity on the single molecular level with the photon-counting histogram. *Biophys J.* 2000;**78**:474–486. [PMC free article] [PubMed]

10. Kask P, Palo K, Ullmann D, Gall K. Fluorescence-intensity distribution analysis and its application in biomolecular detection technology. *Proc Natl Acad Sci USA.* 1999;**96**:13756–13761. [PMC free article] [PubMed]

11. Chen Y, Muller JD, So PT, Gratton E. The photon counting histogram in fluorescence fluctuation spectroscopy. *Biophys J.* 1999;**77**:553–567. [PMC free article] [PubMed]

12. Eggeling C, et al. Data registration and selective single-molecule analysis using multi-parameter fluorescence detection. *J Biotechnol.* 2001;**86**:163–180. [PubMed]

13. Kuhnemuth R, Seidel CAM. Principles of single molecule multiparameter fluorescence spectroscopy. *Single Molecules.* 2001;**2**:251–254.

14. Schwille P, Meyer-Almes FJ, Rigler R. Dual-color fluorescence cross-correlation spectroscopy for multicomponent diffusional analysis in solution. *Biophys J.* 1997;**72**:1878–1886. [PMC free article] [PubMed]

15. Bacia K, Kim SA, Schwille P. Fluorescence cross-correlation spectroscopy in living cells. *Nat Methods.* 2006;**3**:83–89. [PubMed]

16. Meyer T, Schindler H. Particle counting by fluorescence correlation spectroscopy - simultaneous measurement of aggregation and diffusion of molecules in solutions and in membranes. *Biophys J.* 1988;**54**:983–993. [PMC free article] [PubMed]

17. Berland KM, So PTC, Chen Y, Mantulin WW, Gratton E. Scanning two-photon fluctuation correlation spectroscopy: Particle counting measurements for detection of molecular aggregation. *Biophys J.* 1996;**71**:410–420. [PMC free article] [PubMed]

18. Qian H, Elson EL. Analysis of confocal laser-microscope optics for 3-D fluorescence correlation spectroscopy. *Applied Optics.* 1991;**30**:1185–1195.

19. Hess ST, Webb WW. Focal volume optics and experimental artifacts in confocal fluorescence correlation spectroscopy. *Biophys J.* 2002;**83**:2300–2317. [PMC free article] [PubMed]

20. Meakin P. Aggregation kinetics. *Phys Scr.* 1992;**46**:295–331.

21. Goloubinoff P, Christeller JT, Gatenby AA, Lorimer GH. Reconstitution of active dimeric ribulose bisphosphate carboxylase from an unfolded state depends on two chaperonin proteins and Mg-ATP. *Nature.* 1989;**342**:884–889. [PubMed]

22. Lin Z, Rye HS. Expansion and compression of a protein folding intermediate by GroEL. *Mol Cell.* 2004;**16**:23–34. [PubMed]

23. Collins SR, Douglass A, Vale RD, Weissman JS. Mechanism of prion propagation: Amyloid growth occurs by monomer addition. *PLoS Biol.* 2004;**2**:e321. [PMC free article] [PubMed]

24. Shorter J, Lindquist S. Hsp104 catalyzes formation and elimination of self-replicating Sup35 prion conformers. *Science.* 2004;**304**:1793–1797. [PubMed]

25. Patino MM, Liu JJ, Glover JR, Lindquist S. Support for the prion hypothesis for inheritance of a phenotypic trait in yeast. *Science.* 1996;**273**:622–626. [PubMed]

26. Naiki H, Higuchi K, Hosokawa M, Takeda T. Fluorometric determination of amyloid fibrils *in vitro* using the fluorescent dye, thioflavin T1. *Anal Biochem.* 1989;**177**:244–249. [PubMed]

27. Stray SJ, Johnson JM, Kopek BG, Zlotnick A. An *in vitro* fluorescence screen to identify antivirals that disrupt hepatitis B virus capsid assembly. *Nat Biotechnol.* 2006;**24**:358–362. [PubMed]

28. Hagan MF, Chandler D. Dynamic pathways for viral capsid assembly. *Biophys J.* 2006;**91**:42–54. [PMC free article] [PubMed]

29. Pallitto MM, Murphy RM. A mathematical model of the kinetics of beta-amyloid fibril growth from the denatured state. *Biophys J.* 2001;**81**:1805–1822. [PMC free article] [PubMed]

30. Enderlein J, Robbins DL, Ambrose WP, Keller RA. Molecular shot noise, burst size distribution, and single-molecule detection in fluid flow: Effects of multiple occupancy. *J Phys Chem A.* 1998;**102**:6089–6094.
